The Dimanganese(III,IV) Oxidation State of Catalase from *Thermus thermophilus*: Electron Nuclear Double Resonance Analysis of Water and Protein Ligands in the Active Site†

S. Khangulov,‡ M. Sivaraja,‡ V. V. Barynin,§ and G. C. Dismukes*,‡

Department of Chemistry, Hoyt Laboratory, Princeton University, Princeton, New Jersey 08544, and Institute of Crystallography, Academy of Sciences, Moscow, Russia

Received September 29, 1992; Revised Manuscript Received February 19, 1993

ABSTRACT: The ^1H hyperfine tensors of the dimanganese(III,IV) oxidation state of the non-heme-type catalase enzyme from the thermophilic bacterium *Thermus thermophilus* have been measured by electron nuclear double resonance (ENDOR) spectroscopy at pH 6.5–9. These were compared to model dimanganese(III,IV) complexes possessing six-coordinate N_4O_2, N_3O_3, and O_6 atom donor sets to each Mn and μ-oxo and μ-carboxylato bridging ligands. The lack of ^{14}N hyperfine couplings in the enzyme suggests either O_6 or O_5N ligand donors to each Mn. Moreover, the two σ coordination sites on Mn(III) directed at the d_{z^2} orbital cannot be occupied by N ligands. The ^1H ENDOR spectrum revealed two types of anisotropic tensors, attributable to two D_2O-exchangeable protons on the basis of the magnitude of the electron paramagnetic resonance (EPR) line narrowing in D_2O. All six of the ^1H hyperfine couplings are proposed to arise from a single displaceable water molecule in the active site, on the basis of their reversible disappearance, upon incubation in D_2O or by precipitation from ammonium sulfate, and by simulation of the ^1H ENDOR spectrum. The Mn ions are coordinated predominantly by nonmagnetic O atoms lacking covalently bound protons in both α and β positions. This implicates predominantly carboxylato-type ligands (Asp and Glu) and possibly a di-μ-oxo bridge between Mn ions. The latter is supported also by the presence of strong antiferromagnetic coupling. Comparison to other dimetalloproteins also possessing the four-helix bundle structural motif shows that the polyoxo(carboxylato) coordination in catalase differs significantly from the polyhistidine coordination adopted by the diiron(II,II) site in the O_2-binding protein myohemerythrin, but resembles the polycarboxylato ligation adopted by the diiron(III,III) site of ribonucleotide reductase. The catalase ^1H ENDOR spectrum is essentially identical to that for the exchangeable protons in the active site of the diiron(II,III) state of uteroferrin, an acid phosphatase [Doi et al. (1988) *J. Biol. Chem. 263*, 5757–5763], and also for a polycarboxylato complex possessing the $Mn_2(\mu\text{-}O)_2$ core with H-bonded water ligands. The ^1H ENDOR line shape in catalase could be simulated using a theoretical model suitable for multispin clusters. It treats the two Mn spins as point dipoles which are exchange-coupled. It includes both dipolar and isotropic ligand hyperfine couplings. Using this model, the position of the proton with the largest interaction could be located with respect to the Mn–Mn vector because of the extreme sensitivity of line shape to position. Four possible positions are predicted, differing solely by the undetermined sign of the experimental hyperfine tensor elements. Analysis of the ^1H ENDOR spectrum via angle selection using the EPR line shape anisotropy enabled determination of the location of the proton relative to the d_{z^2} orbital of Mn(III), which is orthogonal to the presumed $Mn_2(\mu\text{-}O)_2$ plane. Simulation of the angle-selected ^1H ENDOR spectrum revealed that only one proton position could account for the spectrum. This gives distances of 4.6 and 2.9 Å to Mn(III) and Mn(IV), respectively. These coordinates are compatible with a water or hydroxide molecule H-bonded to a terminal ligand on Mn(IV). A second proton exists at a greater distance. The structural basis for the lack of catalase activity in the Mn_2(III,IV) oxidation state is suggested to originate from the kinetic inertness to substitution or reduction of the bridging oxo atoms in the $Mn_2(\mu\text{-}O)_2$ core.

In addition to the widely distributed heme catalases found in many organisms, a second class of relatively rare occurrence has been identified in *Lactobacillus plantarum* (Kono & Fridovich, 1983a,b; Beyer & Fridovich, 1985) and the extreme thermophile *Thermus thermophilus* (Barynin & Grebenko, 1986; Vainshtein et al., 1984). This enzyme has attracted interest because it utilizes an unusual dimanganese active site which can be interconverted between four redox states. Additionally, it is suspected to exhibit possible functional or structural homology to other polynuclear manganese enzymes such as the bacterial ribonucleotide reductase (Willing et al., 1988) and the photosynthetic water oxidase (Hansson & Wydrzynski, 1990; Brudvig et al., 1989; Dismukes, 1988; Babcock, 1987). A 3-Å X-ray diffraction structure of the *T. thermophilus* enzyme has revealed the principal protein folding elements: six equivalent subunits each folded into a characteristic motif comprising four long antiparallel helices, found in a family of metalloproteins including hemerythrin, apoferritin, cytochromes *c'* and *b*562, tobacco mosaic virus (TMV) coat protein (Vainshtein et al., 1984), and ribonucleotide reductase (Nordlund et al., 1990). In the first four examples and presumably manganese catalase as well, the metal binding site comprises side chains derived from several helices and lies between the interior surfaces of the helices. The structural data on the reduced oxidation state (Vainshtein et al., 1984;

† This research was sponsored by NIH Grant GM-39932.

‡ Princeton University.

§ Academy of Sciences, Russia.

0006-2960/93/0432-4912$04.00/0

Chart I: Protein Coordination in Hemerythrin (A) and Ribonucleotide Reductase (B)[a]

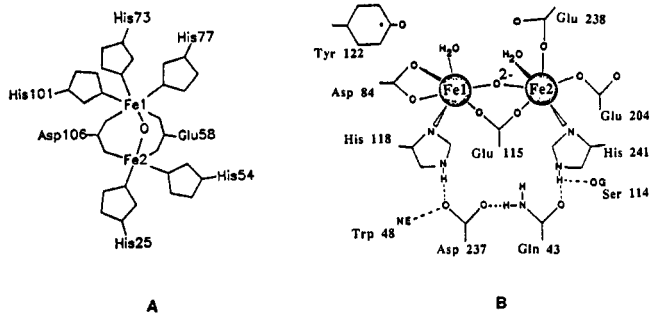

[a] (A) Reprinted with permission from Sieker et al. (1982). Copyright 1982 D. Reidel Publishing Co. (B) Reprinted with permission from Nordlund et al. (1990). Copyright 1990 Macmillan Magazines Limited.

Barynin et al., 1986) place two Mn ions separated by 3.6 ± 0.3 Å within each subunit. An atomic resolution map is still undergoing refinement; hence the coordination of the metal sites remains undetermined. The tertiary structure similarities have led to the speculation that the manganese catalases may also possess coordination environments similar to those found in these related metalloproteins. For example, the reversible O_2-binding protein hemerythrin (Sieker et al., 1982) possesses a diiron(III) site in its oxidized (inactive) form with bridging (μ) oxo and di-μ-carboxylato (Asp and Glu residues) ligands and one terminal aquo and five imidazole ligands (Chart I). Reduction to the Fe(II) state activates the protein for O_2 binding. Only a single iron atom appears to be directly involved in O_2 binding and this undergoes no functional redox change. By contrast, catalase has four redox states involving Mn(II), Mn(III), and Mn(IV) (Khangulov et al., 1986, 1987, 1990a–d; Fronko et al., 1988; Waldo et al., 1991), with strong evidence for catalysis involving Mn_2(II,II) and Mn_2(III,III) oxidation states [Khangulov et al., 1990a,b; reviews, Penner-Hahn (1992) and Dismukes (1992)]. Although these proteins have homologous secondary and tertiary structures, we shall show that Mn catalase is not a simple manganese-containing variant of hemerythrin. This may be responsible in part for their enzymatic differences. Manganese extended X-ray absorption fine structure (EXAFS) (Waldo et al., 1992) and electron paramagnetic resonance (EPR) (Fronko et al., 1988) studies of the "superoxidized" state of *L. plantarum* catalase has revealed a short Mn–Mn distance of 2.67 Å and "multiline"-type EPR signal indicative of the Mn_2(III,IV)(μ-O)$_2$ core. The Mn EXAFS was interpreted to indicate similar protein ligands to Mn in catalase as found for Fe in deoxy hemerythrin (Waldo et al., 1992). However, replacement of both Fe(II) ions by Mn(II), which abolishes the native O_2-binding activity, also failed to induce catalase activity with hydrogen peroxide (D, Kurtz, personal communication). This suggests that the active center of Mn-catalase is unlikely to be the same as the imidazole-containing center of the Mn-substituted hemerythrin.

The present study examines the protein coordination environment of the catalase from *T. thermophilus* as revealed by 9-GHz electron nuclear double resonance (ENDOR) spectroscopy of proton and nitrogen atoms coupled to the ground electronic spin state ($S = {}^1/_2$) of the Mn_2(III,IV) oxidation state. We also report ENDOR hyperfine analysis of the model compound di-μ-oxotetrakis(2,2′-bipyridine)–dimanganese(III,IV) [$Mn_2O_2(bpy)_4(ClO_4)_3 \cdot 2H_2O$] (complex **1**). To extract metrical data, the ligand hyperfine couplings are analyzed using a new theoretical model which describes the dipolar magnetic field surrounding a pair of spin-coupled paramagnetic ions. A computer program based on this theory is used to obtain accurate simulations and from this to deduce the most probable locations of the ^1H nuclei. We have found that this model also describes well the published ENDOR spectra of other spin-coupled dimetalloenzymes, such as uteroferrin.

MATERIALS AND METHODS

Catalase in H_2O (D_2O). The enzyme was isolated and purified by a previously described procedure (Barynin & Grebenko, 1986; Vainshtein et al., 1984). It was stored as a fine crystalline precipitate in 50% saturated ammonium sulfate at 5 °C and redissolved by dialysis against 10 mM phosphate buffer, pH 6.8, to yield concentrated protein solution, 10 mg/mL as determined by spectrophotometry ($\epsilon_{280nm} = 0.95$ mg^{-1} cm^1). As isolated, the protein solution contains no partially occupied Mn sites that could be detected by EPR spectroscopy, but it does possess different oxidation states of the binuclear manganese cluster. The Mn_2(III,IV) oxidation state was generated by oxidation with KIO_4, as described by Khangulov et al. (1986, 1987). This is called the "superoxidized" state of catalase. The same procedure was used to prepare D_2O-enriched Mn(III)Mn(IV) samples. In this case, the buffer, the oxidant and the reductant were prepared in D_2O (99%, Cambridge Isotope Laboratories). D_2O-enriched samples in the Mn(III)Mn(IV) oxidation state were obtained by periodate oxidation of D_2O-exchanged catalase in the Mn_2(II,II) oxidation state.

Catalase in Ammonium Sulfate. The ammonium sulfate precipitate of Mn-catalase in the Mn_2(III,IV) oxidation state was obtained by a procedure similar to that described above. However, the enzyme was maintained in the crystalline precipitate form throughout the entire procedure of oxidation. A 30-μL aliquot of the initial precipitate was loaded in an EPR tube covered by a dialysis membrane. The sample was then reduced by addition of 1 μL of 10 mM hydroxylamine sulfate. Excess hydroxylamine was removed by dialysis against 50% saturated ammonium sulfate. Subsequently, 1 μL of 50 mM potassium periodate was added, and the excess oxidant was removed by dialysis against 50% ammonium sulfate solution.

$Mn_2O_2(bpy)_4(ClO_4)_3 \cdot 2H_2O$. Complex **1a**, which was originally synthesized by Nyholm and Turco (1960), was prepared according to the procedure of Copper et al. (1978) and dissolved in either 50 mM bipyridine buffer, pH 4.6, or 200 mM acetate buffer, pH 4.6, using either H_2O or D_2O as solvent. The final concentration of the complex was 0.5 mM. The pH/pD was adjusted to 4.6 with a solution of glacial acetic acid in H_2O/D_2O. We thank Mr. Peter Pessiki for this sample.

EPR and ENDOR. The X-band EPR spectra were obtained with a Bruker ESP-300 spectrometer operating with a microwave rectangular TE_{102} cavity (ER 4102 ST) and Oxford Instrument ESR-900 continuous-flow cryostat.

ENDOR spectra were recorded at 9.46 GHz in a Bruker ER-250 spectrometer fitted with a cylindrical TM_{110} cavity (EN 801) and 1–30-MHz radiofrequency (RF) coil mounted on the dewar flask. RF power was amplified using an ENI Model 3200 power amplifier. The experiments were performed at 6–10 K using an Oxford ESR-900 cryostat. Typically, the microwave power was 12.8 mW.

ENDOR-Induced EPR. The first-order proton ENDOR spectrum for a single orientation of a paramagnetic center consists of a pair of lines centered at the proton Larmor frequency, $\nu_H = g_H\beta_n H/h$, and split by the angle-dependent

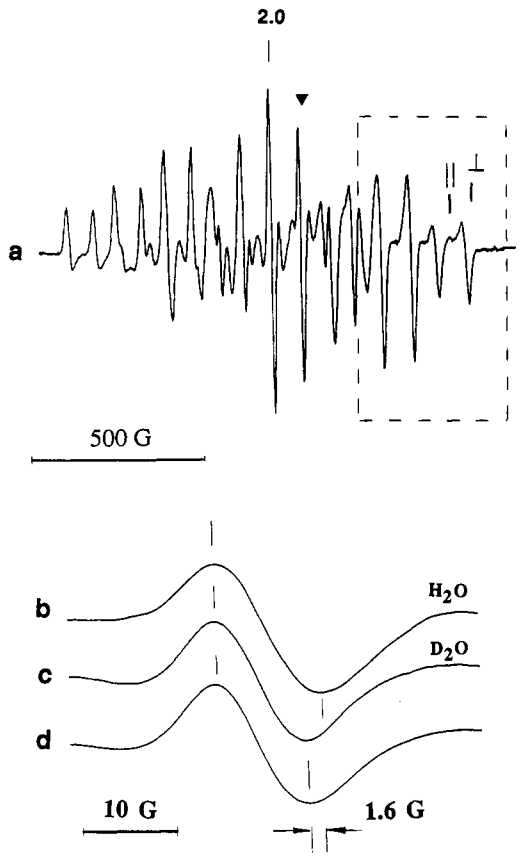

FIGURE 1: (a) EPR spectrum of MnCat(III,IV) as a frozen aqueous solution in H_2O at 35 K. Enlargements of the tenth EPR line (noted by arrowhead) in H_2O (b), D_2O (c), and the microcrystalline precipitate from ammonium sulfate (d) are also shown. Microwave power, 12.8 mW; 100-kHz field modulation, 5 G; time constant, 0.125 s; sweep time, 325 s.

hyperfine coupling constant (A), as given by

$$\nu_{\pm} = |\nu_H \pm A/2| \quad (1)$$

where h is Planck's constant, β_n is the nuclear magneton, and g_H is the nuclear g-factor. To differentiate between multiple overlapping EPR signals giving rise to ENDOR signals, the "ENDOR-induced EPR" (EIE) experiment was performed. This is done by sweeping both the magnetic field and the radiofrequency simultaneously. The radiofrequency varies with magnetic field strength and is set to track the chosen proton resonance, while the magnetic field sweeps out the EPR signal, giving rise to the proton resonance.

RESULTS

EPR. The 9-GHz EPR spectrum of oxidized Mn-catalase, Figure 1, is representative of a well-studied class of mixed-valence Mn_2(III,IV) complexes which typically exhibit 16 resolved ^{55}Mn hyperfine transitions out of the 36 nuclear states which are possible for a dinuclear complex of two spin $I = {}^5/_2$ nuclei. This feature occurs because the Mn hyperfine constants obey the approximate relationship $A_1 = -2A_2$, corresponding to the Mn(III) and Mn(IV) hyperfine constants, respectively (Cooper et al., 1978; Dismukes et al., 1987; Diril et al., 1989; Dismukes, 1990). The spectrum is by far the most well-resolved example known of the class, including all synthetic model complexes. The narrowness of the line width attests to the lack of appreciable strain in the hyperfine and g tensors and thus indicates a high degree of uniformity to the coordination environments of the Mn ions.

The overall line shape of the EPR spectrum of catalase in D_2O is the same as that in H_2O. The individual lines narrow slightly by about 1.3 ± 0.3 G upon D_2O exchange, as shown in Figure 1b. This narrowing arises from the presence of unresolved hyperfine interactions with exchangeable protons and the 6.5-fold smaller magnetic moment of deuterium. Resolution of these proton couplings can be observed in the ENDOR experiment.

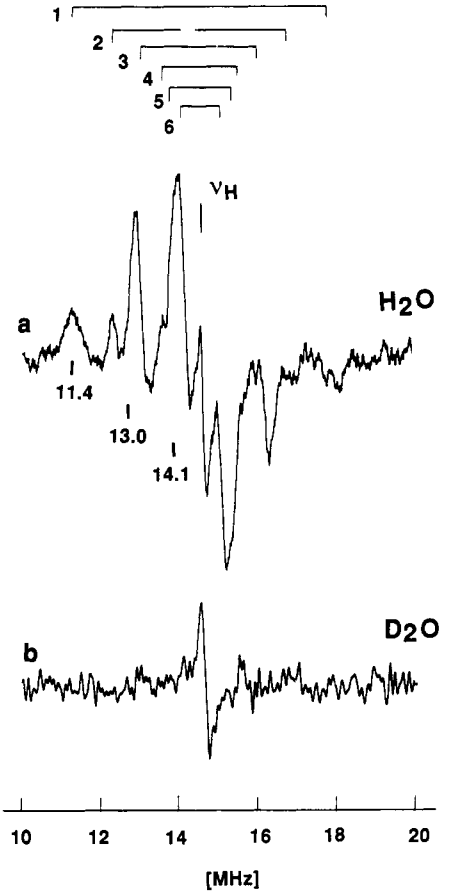

FIGURE 2: ^1H ENDOR spectra of Mn-catalase in the Mn_2(III,IV) state at magnetic field H_0 = 3436 G (noted by arrowhead in Figure 1) in (a) H_2O buffer and (b) D_2O buffer. ENDOR conditions: microwave frequency, ν_0 = 9.45 GHz; microwave power, 32 mW; time constant, 372 ms; sweep time, 83 s; time constant, 372 ms; modulation frequency, 12.5 kHz; modulation depth, 100 kHz; number of scans, 32.

Table I: ^1H ENDOR Hyperfine Splittings[a] for Mn-Catalase, Uteroferrin, and Dimanganese Compounds

	1a	**1b**[b]	Mn-catalase	uteroferrin[c]
1	8.3	6.2	6.6	6.0
2	4.7	4.9	4.5	4.2
3	2.3	3.6	3.3	3.5
4	1.0	2.8	2.0	1.9
5		2.1	1.4	1.3
6		1.2	0.8	1.0
field (G)	3355	3355	3436	3864

[a] Hyperfine splittins are given in megahertz. [b] Complex **1b** is complex **1a** dissolved in 0.2 M acetate buffer. [c] Data from Doi et al. (1988).

ENDOR of Catalase in H_2O. Figure 2 shows the proton ENDOR spectrum of Mn-catalase in the Mn_2(III,IV) state measured at the center of the EPR signal (3436 G). The spectrum in Figure 2a has a pattern that is symmetric about ν_H, exhibiting at least six resolved pairs of resonances ranging from 0.8 to 6.6 MHz, Table I. The pattern shifts linearly with field in accordance with ν_H (data not shown), confirming that these peaks arise from protons. The narrow matrix peak centered at ν_H arises from weakly coupled distance protons. At the observing Zeeman field of 3436 G, several overlapping

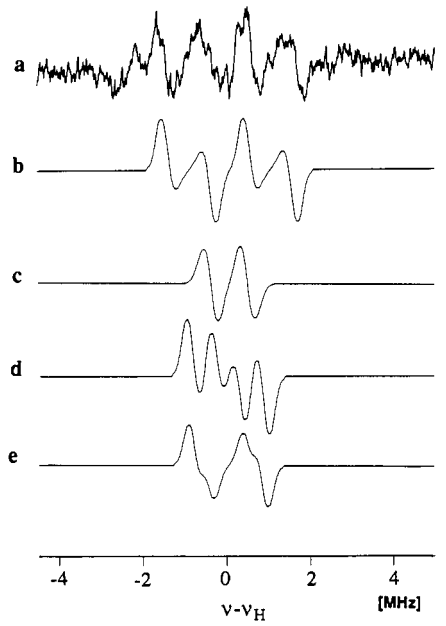

FIGURE 3: (a) ^{1}H ENDOR spectrum of catalase at the perpendicular turning point (3904 G) of the EPR signal (Figure 1a). The central matrix peak has been subtracted (b–e) in the simulated ^{1}H ENDOR spectra at the perpendicular turning point of the EPR signal. Simulated spectra correspond to different positions of the hydrogen atom relative to the Mn(III)–Mn(IV)–vector, as shown in Chart IV. (b) Case I(b); (c) case I(a); (d) case II(b); (e) case II(a).

EPR transitions are irradiated and all orientations of the molecule with respect to the static field contribute to the EPR intensity. Hence the ENDOR spectrum should be a powder pattern, and this is indeed observed. The symmetry and polarity of the peaks is reversed on either side of the matrix peak. These features are typical of the powder pattern of a system with anisotropic hyperfine tensors possessing principal components with opposite signs (Kurreck et al., 1988). From the spectrum it is not obvious how many different types of protons contribute to the pattern.

In order to simplify analysis of the spectrum, we performed ENDOR at field positions corresponding to turning points of nondegenerate ^{55}Mn nuclear states in the outer extremes of the EPR spectrum. This should give rise to single crystal-like ENDOR patterns (Rist & Hyde, 1970). The outer transition is resolved into parallel and perpendicular turning points, as noted in Figure 1a. The ^{1}H ENDOR spectrum obtained at the perpendicular EPR turning point is of much weaker intensity, yet it clearly reveals two pairs of lines at the same positions as the 0.8- and 3.3-MHz couplings observed when irradiation is performed on the central EPR peaks (Figure 3a). There is no evidence for the largest coupling of 6.6 MHz when irradiation is performed on the perpendicular EPR turning point. This result is consistent with an assignment to one or more anisotropic tensors (Zheng & Dismukes, 1992). According to our simulation of the EPR spectrum, the EPR intensity at this point arises from molecules oriented with the principal axis of the Mn(III) hyperfine tensor (along the d_{z^2} orbital) oriented perpendicular to the applied magnetic field, i.e., the field is in the plane of the proposed $Mn_2(\mu\text{-}O)_2$ rhombus. At the unique parallel turning point of the EPR signal, the ^{1}H ENDOR effect was too weak to observe.

We also examined the pH dependence of both the EPR and ^{1}H ENDOR spectra in the range 6.5–9.0 (not shown). Neither spectrum changed, indicating that the pK_a of the observed protons is above this pH range.

ENDOR of Catalase in D_2O. Figure 2b shows the proton ENDOR region for the Mn_2(III,IV) state of catalase in D_2O.

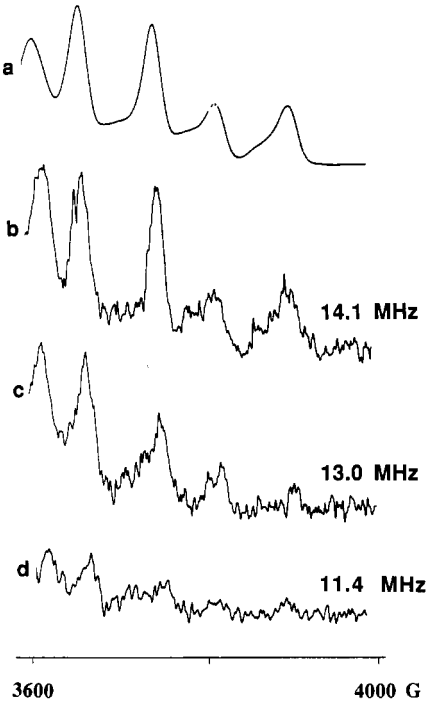

FIGURE 4: (a) High-field part of the catalase EPR absorption spectrum (framed region in Figure 1a). Traces b, c, and d give the ^{1}H ENDOR-induced EPR signals arising from three different ^{1}H ENDOR lines. At 3436 G these ENDOR transitions are at (b) 14.1, (c) 13.0, and (d) 11.4 MHz. These positons correspond to three ENDOR lines pairs marked in Figure 2a.

It is clear that D_2O exchange abolishes all the resolved proton couplings and only the matrix peak remains. This indicates that all the resolved proton couplings belong to exchangeable protons. This is consistent with the narrowing of the EPR line width in Figure 1. The exchanged protons show up as broad deuterium resonances in the ENDOR spectrum in the 1–2-MHz region, as expected for the 6-fold smaller magnetic moment (data not shown). Quantitative analysis of the deuteron spectrum was not attempted.

Catalase in Ammonium Sulfate. The ammonium sulfate microcrystalline precipitate of the Mn(III)Mn(IV) state of catalase obtained from H_2O solutions yields an EPR spectrum identical to that observed in frozen D_2O solutions without precipitation by ammonium sulfate (not shown). Surprisingly, the individual lines are narrowed to the same extent as was observed by D_2O exchange in solution (Figure 1b). The reason for this is revealed by the ^{1}H ENDOR spectrum of the microcrystalline sample obtained from H_2O. It is identical to the solution spectrum obtained in D_2O, shown in Figure 2b. It exhibits only the matrix peak and none of the resolved ^{1}H couplings that are observed in the frozen solution spectrum in H_2O (data not shown). Evidently the D_2O-exchangeable protons are also removed simply by ammonium sulfate precipitation from H_2O. This suggests that all of the resolved protons are associated with water (or hydroxide) molecules bound near the manganese ions, which may be displaced by sulfate or by ammonia, or possibly by protein residues which may be ionized by NH_3. We disfavor the interpretation that water is replaced by ammonia, since this should lead to observable ^{1}H resonances, which we do not see.

^{1}H ENDOR-Induced EPR of Mn-Catalase. We performed the ^{1}H EIE experiment for two reasons: first, to check if the observed ENDOR pattern is in fact from a single paramagnetic species, and second, to see if by irradiating different ENDOR peaks we could obtain angle-selected EPR signals. Figure 4 shows part of the EIE signal between 3600 and 4000 G from

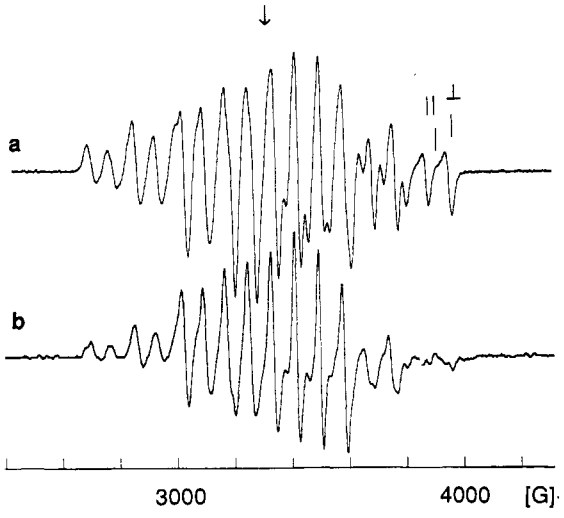

FIGURE 5: EPR spectra of complex **1a** dissolved in 50 mM bipyridine buffer, pH 4.6 (a), and 0.2 M acetate buffer, pH 4.6 (b), at 40 K.

three ENDOR lines with proton frequencies (at H_0 = 3436 G) of (b) 14.1, (c) 13.0, and (d) 11.4 MHz, corresponding to hyperfine splittings of 0.8, 3.3, and 6.6 MHz, respectively (Table I). These lines are indicated in Figure 2a. The EIE spectra are compared with the conventionl EPR absorption signal in Figure 4a, obtained by integration of the experimental spectrum (see framed region in Figure 1a). The EPR absorption and EIE signals are indistinguishable within the sensitivity of the experiment at two of the three pump frequencies, indicating that these proton ENDOR lines arise from a single Mn_2(III,IV) species. The EIE signal at 11.4 MHz is too weak to discern the line shape.

^{14}N ENDOR of Mn(III)Mn(IV) Catalase. Using the electron spin-echo envelope modulation technique (ESEEM) to examine the Mn(III)Mn(IV) catalase state, Dikanov et al. (1988) observed coupling to a single class of ^{14}N nuclei. They assigned an isotropic hyperfine coupling of 2.3 MHz and a quadrupolar coupling of $|e^2Qq|$ = 2.4 MHz. Because of this precedent, we looked closely for ^{14}N ENDOR signals in the Mn_2(III,IV) catalase sample but were unable to detect any signal. The reason for this difference may be that the ESEEM technique is more sensitive for detecting weak hyperfine modulations from anisotropic nuclei like ^{14}N than is the ENDOR technique. However, as will be shown below, we were able to detect strong ^{14}N resonances from complex **1a** at the same concentration as catalase. Using this as an approximate intensity standard, we were able to limit the number of possible N ligands to $\leq$ 1 N/Mn.

^1H ENDOR Spectra of Complex 1. Figures 5a and 6a show the EPR and ^1H ENDOR spectra, respectively, of **1a** in bipyridine/H_2O buffer. The 16-line EPR spectrum of **1a** has been well studied, and assignment of the isotropic ^{55}Mn hyperfine structure is known (Copper et al., 1978). The ^1H ENDOR spectrum has at least four well-resolved pairs of lines with hyperfine constants of 8.3, 4.7, 2.3, and 1.0 MHz, listed in Table I. Unlike the anisotropic line shape of catalase, the line shape of **1a** exhibits a derivative shape typical of nearly isotropic couplings. Replacement of H_2O with D_2O in the buffer and incubation for up to 12 h does not noticeably affect the ENDOR spectrum (data not shown), indicating that all the proton couplings belong to nonexchangeable protons. These protons must therefore come from the bipyridine ligands. Because the proton couplings in catalase and **1a** differ in all respects, we conclude that the chemical origin of the protons is different.

Dissolving **1a** in 0.2 M acetate buffer changes the EPR spectral line width yet gives little change in the average ^{55}Mn hyperfine constants; compare Figure 5b to 5a. By contrast, this yields a dramatic change in both the ^1H and ^{14}N ENDOR spectra. All ^{14}N resonances described in the following section disappear, while the ^1H spectrum changes to that given in Figure 6b. Now the ^1H spectrum is represented by six pairs of lines with hyperfine splittings of 6.2, 4.9, 3.6, 2.8, 2.1, and 1.2 MHz. The line shape in this case becomes anisotropic, similar to that seen in the catalase ^1H spectrum and unlike the derivative-type line shape of **1a** in bipyridine buffer. The hyperfine couplings are very similar to those in Mn-catalase. Moreover, the ^1H ENDOR spectrum of **1a** dissolved in acetate buffer now becomes sensitive to D_2O substitution; replacement of H_2O by D_2O diminishes all of the ^1H ENDOR peaks, as seen in Figure 6c. This is analogous to the ^1H ENDOR spectrum of catalase. Thus, the ^1H ENDOR results suggest that most or all ENDOR-detected bipyridine ligands of **1a** are replaced by acetate or aquo ligands upon incubation in 0.2 M acetate buffer, as proposed by the following equilibrium:

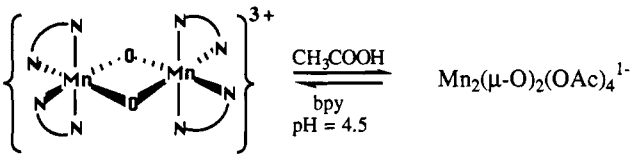

1a **1b**

^{14}N ENDOR of Complex 1a. As shown in Figure 7a, complex **1a** exhibits four strong ENDOR lines labeled pp′ and qq′ in the 4–10-MHz range and several weaker features in the 1–4-MHz region when an EPR transition is monitored on any of the central peaks given in Figure 5a. Because **1a** possesses trapped valences for Mn(III) and Mn(IV), there are four chemically nonequivalent N coordination sites corresponding to axial and equatorial positions relative to the Mn_2O_2 plane. One of these classes, which we term the π class, was observed by Britt et al. (1989) using ESEEM spectroscopy. Assuming an isotropic hyperfine interaction, they reported a hyperfine constant of $A(^{14}N)$ = 2.8 MHz and a quadrupole moment of $|e^2Qq|$ = 2.3 MHz. This class of nitrogens should yield four ENDOR transitions at frequencies determined by $|A/2 \pm {}^3/_4e^2Qq \pm \nu_n|$. At 3355 G these should occur at 0.7, 1.4, 2.1, and 4.2 MHz, which may be responsible for the cluster of weak overlapping transitions observed between 1 and 4 MHz in Figure 7a.

The four well-resolved and intense ENDOR resonances in the 4–10-MHz region of Figure 7 were not observed in the ESEEM study. They belong to one or more additional classes of nitrogens, with larger hyperfine coupling constants. To aid in assigning these peaks, we examined their orientation dependence by setting the magnetic field at the outer parallel and perpendicular turning points of the EPR spectrum, as noted in Figure 5a. Two of the four ENDOR transitions labeled pp′ are observed only in the perpendicular position (Figure 7b), while the qq′ pair appear only in the parallel position (Figure 7c). From this we conclude that the four transitions belong to orthogonal tensor components of the same class of nitrogens rather than to different nitrogens. The magnetic field dependence, summarized in Table II, indicates that these peaks can be attributed to ^{14}N transitions and associated into two pairs, pp′ and qq′, each split by 2 ν_n. The centers of each pair do not change appreciably with magnetic field between 3060 and 3980 G, as expected if determined by hyperfine and/or quadrupole interactions.

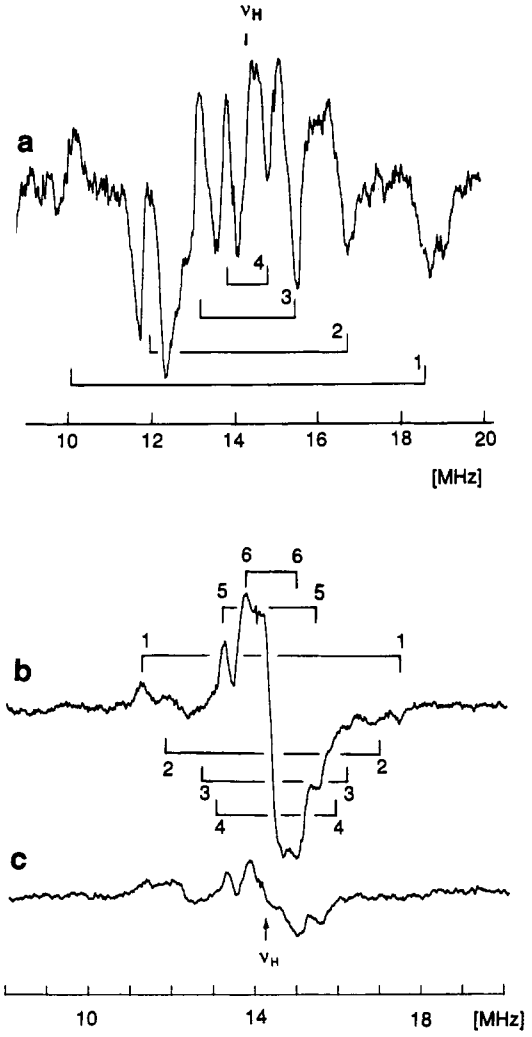

FIGURE 6: ^{1}H ENDOR spectra of complex **1a** dissolved in 50 mM bipyridine buffer (pH 4.6), H_0 = 3288 G (a), and in 0.2 M acetate buffer, pH 4.6, (b) in H_2O and (c) in D_2O.

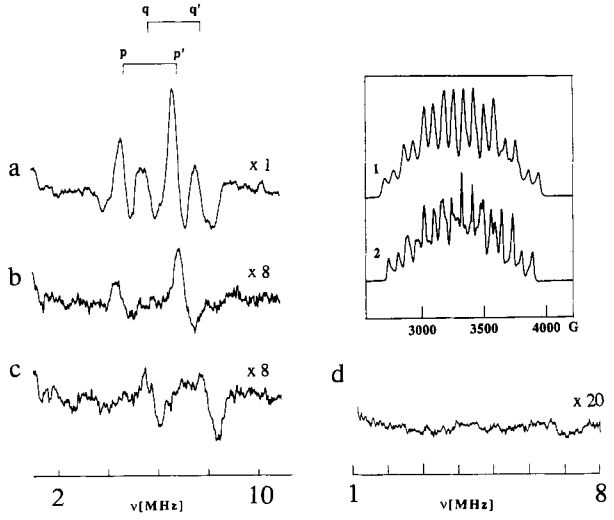

FIGURE 7: ^{14}N ENDOR spectra of complex **1a** at (a) 3355 G, (b) 3950 G, and (c) 3982 G. These fields correspond to positions noted in Figure 5a at the center (↓), ⊥, and ∥, respectively. Trace d shows the lack of ENDOR transitions from 1 to 8 MHz for MnCat(III,IV), even though the integral of the EPR signal intensity is equal to the EPR intensity of complex **1a** (compare curves 2 and 1, respectively, in inset).

The ^{14}N ENDOR spectra in Figure 7 could be explained by the following first-order hamiltonian, applicable to the

Table II: Magnetic Field Dependence of ^{14}N ENDOR Transitions[a] for Complex **1a**

H^b (G)	$\nu_{p'} - \nu_p$	$\nu_{q'} - \nu_q$	$2\nu_n$	$(\nu_{p'} + \nu_p)/2$	$(\nu_{q'} + \nu_q)/2$
3060	1.8	1.8	1.88	5.7	6.5
3355 (↓)	2.0	2.1	2.07	5.8	6.8
3710	2.2	2.1	2.28	5.6	6.7
3950 (∥)	no	2.4	2.43	no	6.9
3982 (⊥)	2.5	no	2.45	5.8	no

[a] ENDOR transitions are given in megahertz. [b] See Figure 5a.

Chart II: ^{14}N ENDOR Stick Spectrum for Figure 7

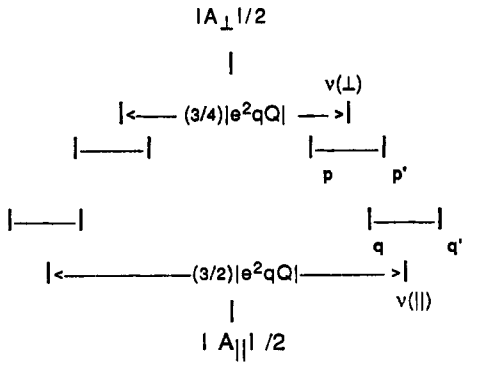

case of a magnetic field applied at an angle θ relative to collinear hyperfine and quadrupole tensors possessing axial symmetry (Abragam & Bleaney, 1970; eqs 3.54 and 3.61):

$$H = g_e\beta_e H_z S_z - g_n\beta_n H_z I_z + {}^3/_4|e^2qQ|[I_z^2 - I(I+1)/3] + AI_zS_z \quad (2)$$

We have taken the electron g_e value to be isotropic as found from simulation of the EPR signals of *L. plantarum* (Vanngard et al., 1992) and *T. thermophilus* (Zheng & Dismukes, 1992). The nuclear g_n value is isotropic and $\nu_n = g_n\beta_n HM_I$. The application of eq 2 requires $A \gg |e^2qQ|$ and ν_n. The magnetic hyperfine and nuclear quadrupole parameters in eq 2 are defined by, respectively,

$$A^2 = A_\parallel^2 \cos^2\theta + A_\perp^2 \sin^2\theta$$

$$P = ({}^3/_8)|e^2qQ|[(A_\parallel^2/A^2)(3\cos^2\theta) - 1]$$

For a ^{14}N nucleus the first-order predicted ENDOR frequencies can be found from the following equations (Abragam & Bleaney, 1970; eqs 3.62 and 4.4):

$$\nu_{ENDOR}(\Delta M_I = +1) = |-\nu_n + P \pm A/2| \quad (3a)$$

$$\nu_{ENDOR}(\Delta M_I = -1) = |-\nu_n - P \pm A/2| \quad (3b)$$

For any angle θ, eq 3 describes a four-line pattern centered at $A/2$, consisting of two pairs of Larmor split doublets, each split by the quadrupolar term. For a randomly oriented sample, a powder line shape is expected with resonances at the extreme turning points $\theta = 0$ and $\pi/2$. Thus, as many as eight peaks could be expected for axial tensors. The orientation selection we observe for the experimental ^{14}N ENDOR spectrum at the turning points of the EPR signal (Figure 5, ↓, ∥, and ⊥) is explained well by eq 3, as depicted by the stick spectrum in Chart II. The peaks labeled pp′ and qq′ are predicted to be the high-frequency pairs arising from molecules oriented either parallel or perpendicular, respectively, to coaxial ^{14}N hyperfine and quadrupole tensors. The four lower frequency partners predicted to accompany the transitions

Table III: ^{14}N Hyperfine and Quadrupole Coupling Constants[a] for Dimanganese(III,IV) Clusters and Catalase

	α[b]	$\lvert A\rvert$[b]	$\lvert e^2Qq\rvert$	ref, method
$[Mn_2(CYCLAM)_2O_2](ClO_4)_3$[c]		9.2	2.98	Tan et al. (1991), ENDOR
$[Mn_2(TMPA)_2O_2](ClO_4)_3$[d]		11.2	3.02	Tan et al. (1991), ENDOR
complex **1a**	0.1	10.8	2.0, 1.5	this work, ENDOR
	0.0	9.4	2.9	
	−0.1	8.3	3.8, 4.0	
complex **1a**		2.8	2.3	Britt et al. (1989), ESEEM
$Mn_2(HBPz_3)O_2(\mu\text{-}CH_3CH_2CO_2)$[e]		3.8, 4.4, 5.0, 5.3, 5.9[e]		Baumgarten et al.,[f] ENDOR
Mn-catalase		2.3	2.44	Dikanov et al. (1988), ESEEM

[a] Coupling constants are given in megahertz. [b] $\alpha = (|A_\perp| - |A_\parallel|)/|A|$. [c] CYCLAM = 1,4,8,11-tetraazacyclotetradecane. [d] TMPA = Tris(2-methylpyridyl)amine. [e] $HBPz_3$ = hydrotris(pyrazolyl)borate. Observed ^{14}N transition frequencies at 3940 G. [f] Baumgarten, Sheats, and Dismukes, unpublished results.

pp′ and qq′ should occur in the 1–4-MHz region. These should be much weaker since now the internal magnetic field is comparable to the Zeeman field and the axis of quantization is undetermined. Moreover, these low-frequency transitions should overlap with the previously noted π-type class of weakly coupled nitrogen ligands.

For the case when the ^{14}N hyperfine interaction is mainly determined by the isotropic Fermi contact mechanism (i.e., $A_\parallel/A_\perp \approx 1$), we can estimate the magnetic hyperfine and quadrupolar interaction constants using the following equations (see also Chart II):

$$\nu(\parallel) = (\nu_q + \nu_{q'})/2 = |A_\parallel|/2 + {}^3/_8|e^2qQ|\{3(A_\parallel{}^2/A_\perp{}^2) - 1\}$$

$$\approx |A_\parallel|/2 + {}^3/_4|e^2qQ| \quad (4a)$$

$$\nu(\perp) = (\nu_p + \nu_{p'})/2 = |A_\perp|/2 + {}^3/_8|e^2qQ| \quad (4b)$$

Relating these equations to the experimental values for $\nu(\parallel)$ and $\nu(\perp)$ enables a useful empirical relationship to be expressed between the anisotropy, $\alpha = (|A_\perp| - |A_\parallel|)/|A|$, the isotropic hyperfine constant, $|A| = (2|A_\perp| + |A_\parallel|)/3$, and $|e^2qQ|$. For small α the latter parameters are $|e^2qQ|$ (MHz) = $2.93 - 12.6\alpha - 15.9\alpha^2$ and $|A|$ (MHz) = $9.15 - 0.56|e^2qQ|$. This gives, for the isotropic case ($\alpha = 0$), $|A| = 9.4$ MHz and $|e^2qQ| = 2.92$ MHz. If the hyperfine interaction is also anisotropic, only the range of allowed values for A and e^2qQ which satisfy the spectrum can be given. For 10% anisotropy in α, the parameter values listed in Table III are found. The case with an isotropic A gives values that are in good agreement with the (assumed) isotropic ^{14}N hyperfine interaction and quadrupolar tensor reported for the analogous $Mn_2(III,IV)(\mu\text{-}O)_2$ complexes prepared using CYCLAM and TMPA terminal ligands, as listed in Table III (Tan et al., 1991).

Because angle selection is performed using the tensor(s) responsible for the EPR anisotropy, we see that the result noted above places the direction of the principal axis of the axial ^{14}N quadrupole tensor of complex **1a** close to the EPR tensor. On the basis of simulation of the EPR signal, the anisotropy arises predominantly from the Mn(III) hyperfine tensor (30%) and much less from the Mn(IV) hyperfine anisotropy (10%) of g anisotropy (<0.3%) (Vanngard et al., 1992; Zheng & Dismukes, 1992). Consequently, the Mn(III) hyperfine tensor is close to coaxial with the ^{14}N hyperfine tensor. This result is expected for N ligands bound to Mn(III) along the axis bearing the lone antibonding d electron (axial site). The crystal structure of complex **1a** exhibits a long N–Mn(III)–N bond perpendicular to the $Mn_2(\mu\text{-}O)_2$ plane, which can be identified with the d_{z^2} orbital bearing the antibonding unpaired electron (Stoufer & Palenik, 1972).

DISCUSSION

Origin of ^1H Hyperfine Coupling. The EIE data of Figure 4 show that all six proton couplings evident in Figure 2 originate from the $Mn_2(III,IV)$ state of catalase. Because all resolved proton couplings are exchangeable in D_2O, we may eliminate from consideration protein residues which have nonexchangeable protons in the α or β position next to the coordinating atom. This rules out the amino acids cysteine, serine, threonine, and lysine. As summarized below, we were able to restrict the maximum number of ^{14}N ligands (histidine?) to ≤1 N/Mn on the basis of comparison with model complexes having N_4O_2 and O_6 coordination. This leaves only carboxylate residues such as Asp and Glu as candidates for the majority of protein ligands, since these have no protons at α or β sites. Thus all of the exchangeable protons in catalase may be restricted to either Mn-coordinated histidines (≤1 N/Mn) or H-bonded water (or hydroxide) or polar amino acid molecules which donate protons to either Mn-coordinated carboxylato or bridging oxo ligands. The elimination of all resolved ^1H ENDOR splittings by precipitation of the protein from ammonium sulfate solutions strongly favors the possibility that all protons are derived from labile H-bonded water or hydroxide molecules. Foreshadowing this observation, anions are known to bind to the active site of the $Mn_2(II,II)$ oxidation state of catalase (Khangulov et al., 1987).

The proton ENDOR couplings, line shape, and exchangeability in D_2O for Mn-catalase (Figure 2) are almost identical to those for complex **1b** (Figure 6b,c). This argues strongly in favor of polycarboxylato coordination for Mn-catalase. Water molecules are not able to form H-bonds with the first-shell ligand atoms to the Mn site of **1a**, but water accessibility is increased by replacing the terminal hydrophobic bipyridine ligands by hydrophilic acetate ligands.

The proton ENDOR pattern of Mn-catalase is very similar to that of the Fe(II)Fe(III) site in the dimetalloenzyme uteroferrin, for which D_2O exchange also replaces the major ^1H resonances (Doi et al., 1988) (Table I). There is also direct crystallographic evidence for water coordination to the ferric ions of the diiron(III) site of ribonucleotide reductase, as illustrated in Chart I (Nordlund et al., 1990). Both pieces of evidence indirectly support the idea that the exchangeable proton ENDOR signals in Mn-catalase might originate from H-bonded water or hydroxide molecules.

Proton Stoichiometry from EPR Line Width. There is a quantitative relationship between EPR line width and unresolved hyperfine couplings which allows an accurate estimation of the number of magnetic nuclei contributing to the EPR line width. The expression for the derivative EPR line width (ΔH_G) arising from a distribution of unresolved isotropic hyperfine splittings was used (Lebedev & Muromtcev, 1972):

$$\Delta H_G = (2/(3)^{1/2})[\sum_{c=1}^{n} a_n^2 I_n(I_n + 1)]^{1/2}$$

We used this expression to estimate how many protons are responsible for the average 1.3 ± 0.3 G EPR line narrowing (Figure 1b) observed upon exchange with D_2O (Figure 1b illustrates the maximum narrowing observed). Taking each proton to contribute a mean hyperfine coupling equal to $a = {}^1/_3(|A_x| + |A_y| + |A_z|)$ and choosing the intense group of three ^{1}H ENDOR couplings at 6.6, 3.3, and 0.8 MHz as the elements of the same hyperfine tensor (Table I), the average number of protons needed to reproduce the experimental line narrowing is predicted to be $N = 1.4 \pm 0.4$. The experimental ENDOR spectrum includes another class of protons having weaker intensity with resolved hyperfine splittings of 4.5, 2.0, and 1.4 MHz (Table I). If these are due to the elements of a second tensor, the predicted line broadening of the EPR signal if one proton from each of these classes is present is equal to 1.5 G. From this we conclude that the ^{1}H ENDOR couplings are only consistent with the the existence of two protons, one from each class, as the source of the D_2O-exchangeable EPR line broadening. Attempts to explain the EPR line narrowing in D_2O using the six ENDOR hyperfine frequencies and assuming greater than two protons always predicted too large a narrowing.

Other reasons which argue in favor of assigning the three most intense ^{1}H ENDOR peaks to a single class of protons (only one proton in the class) as follows: (1) all three peaks are independent of pH from 6.5 to 9.5 ($pK_a > 9.5$), (2) all exchange with D_2O at rates faster than 12 h, the shortest incubation time used, (3) all are lost upon incubation in $(NH_4)_2SO_4$—we saw no differential loss of one peak over another, and (4) the ENDOR line shapes of the three peaks responded equally to changes in temperature between 6 and 18 K and to changes in microwave power from 12 to 205 mW. These observations, taken together, suggest that a single water molecule may be responsible for all of the proton ENDOR signals.

Could histidine ligands to Mn account for the ^{1}H ENDOR signal? A single histidine is a candidate for Mn ligation on the basis of the ESEEM results of Dikanov et al. (1988). Histidine has a proton on the ϵ-carbon atom between the nitrogen atoms and also one on the δ-carbon, which might be observable by ENDOR. The proton of the δ-carbon should be nonexchangeable with D_2O under our conditions, while the proton on the δ-nitrogen is acidic and should readily exchange. The ϵ-carbon is weakly acidic and may possibly undergo exchange. Unfortunately, there are no hyperfine data we are aware of for model Mn(III) or Mn(IV) complexes using histidine or imidazole ligands. For comparison, the ^{1}H hyperfine constants reported for imidazole coordinated to the π site on low-spin $Fe^{III}(TPP)(Im)_2^+$ occur in the range which we observe for protons interacting with Mn-catalase (MHz): 3.5–3.7 (C-2), 1.2 (N-3), ~0 (C-4), and 2.7–4.8 (C-5) (Scholes et al., 1982, 1986). Since these values are believed to be largely dipolar in nature, the proper scaling factor to use to extrapolate these values to a spin-coupled Mn_2(III,IV) center is $S_i \cdot S/S^2$. This scaling is +2 and −1 for Mn(III) and Mn(IV), respectively. This extrapolation must be used with caution, as it is valid only if the ligand hyperfine interaction occurs predominantly to one of the Mn ions in the dimer. Ligand dipolar hyperfine coupling to both Mn ions, as would occur if the ligand were occupying a bridging site between Mn ions, could lead to a diminished interaction owing to the antiferromagnetic orientation of the electron spins. The C-4 imidazole proton in the low-spin heme system exhibits no observable coupling, and this could also hold true for Mn coordination. The C-5 (δ) position would be bound to the β-carbon in histidine, so there is no proton at this site. One of the two protons on the β-carbon could exhibit a dipolar coupling as large as that for the N-3 proton, but it could also be less, depending on the conformation of the Cα–Cβ bond. This analysis suggests that as few as two labile ring protons at N-3 (δ) and C-2 (ϵ) and possibly one or two nonlabile protons at Cβ could have observable hyperfine tensors to Mn(III) or Mn(IV). An N-3 (δ) proton would possess an even smaller hyperfine splitting if it were strongly H-bonded, which could therefore be difficult to resolve. Experimentally, we see only six hyperfine splittings for catalase whose magnitudes and exchangeability are compatible with C-2 and N-3 histidine protons but not with Cβ.

We do not expect histidine protons to be eliminated by precipitation of the protein from ammonium sulfate, as we observe, unless dissociation of Mn-bound histidine occurs. This seems improbable since the EPR spectrum is not perturbed other than the noted line width narrowing. Thus we conclude that hyperfine splittings to histidine protons are not resolved in our ENDOR data. This may be reconciled with the weak ^{14}N hyperfine interaction reported by Dikanov et al. (1988) if this is due to a dipolar coupled N atom H-bonded to a Mn oxygen ligand, rather than directly coordinated to Mn.

Chemical Identity of the N Ligand in Mn Catalase. The N ligand bound to Mn in catalase observed in the ESEEM data of Dikanov et al. (1988) was reported to have a hyperfine constant of $A(^{14}N) = 2.3$ MHz. They hypothesized that this could be due to the amino nitrogen of an imidazole group and suggested that the directly coordinated imino nitrogen to Mn should have a much larger hyperfine coupling constant of ≥9 MHz, which would render it unobservable in their ESEEM experiment. For catalase we could not detect any ^{14}N ENDOR resonances above 3 MHz, where the ENDOR technique is more sensitive than ESEEM. Hence the remote N-histidine proposal by Dikanov is not supported. We were able to place an upper limit on the number of N ligands which could go undetected in our ENDOR analysis of catalase by comparison with the multiple N resonances observed in complex **1a** and its product in acetate buffer **1b** (Figures 6 and 7 and Table I). This indicates that catalase has no σ-type N ligands and ≤1 N/Mn of π type.

From ^{14}N ESEEM (Britt, 1988) and our ENDOR results on complex **1a** it is clear that the hyperfine couplings for aromatic nitrogen ligands coordinated to Mn(III) and Mn(IV) fall in the range 2.8–12 MHz. Comparing our data for **1a** with ^{14}N ENDOR data reported by Tan et al. (1991) for $[Mn_2(CYCLAM)_2O_2](ClO_4)_3$ and $[Mn_2(TMPA)_2O_2](ClO_4)_3$ enables us to make a more specific assignment of the possible stereochemical origin of the ^{14}N resonance reported by Dikanov et al. (1988). The ^{14}N hyperfine constants of nitrogen ligands coordinated to Mn_2(III,IV) dimers fall into two ranges. Large couplings in the range 7–11 MHz occur at the Mn(III) sites having σ symmetry with respect to the lone antibonding d_{z^2} orbital (structure **2**):

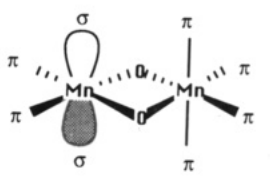

2

From crystallographic studies of complex with the $Mn_2O_2^{3+}$

core, this is located perpendicular to the plane of the Mn_2O_2 rhombus (Stoufer & Palenik, 1972; Wieghardt, 1989). Much smaller couplings, <3 MHz occur at equatorial coordination sites which have only π interactions with the unpaired electrons. All sites on octahedrally coordinated Mn(IV) can have only π interactions, since the d electronic configuration is t_{2g}^3. Thus, small ^{14}N hyperfine interactions are predicted. Therefore, the small 2.3-MHz ^{14}N hyperfine of catalase reported by Dikanov et al. (1988) could actually be from a nitrogen directly coordinated to Mn(IV) or to a π site on Mn(III) rather than the remote N of a histidine ligand bound to a σ site. However, as noted in the previous section, a π-type terminal histidine ligand appears to be incompatible with the lack of nonexchangeable proton couplings. We propose a tentative hypothesis that the ^{14}N coupling originates from a H-bonded protein residue, possibly from histidine, which is not directly coordinated to Mn. If this were to occur to a μ-oxo bridge or to a σ-site oxygen ligand bound to Mn(III) where the spin density should be highest, the 2.3-MHz ^{14}N hyperfine coupling might be reconciled. An answer to this question could come from hyperfine measurements of histidine–Mn(III) and –Mn(IV) complexes. An intriguing hypothesis is that the N coupling may originate from the proton donor with $pK_a = 5.5$ which has been identified in the reduced enzyme as essential for catalase activity (Khangulov et al., 1990a,c).

Quantitative Metrical Analysis of Ligand Proton Coordinates from Hyperfine Interaction with a Spin-Coupled Mn Pair. For a powder pattern line shape, in principle all six observed turning points in the ^1H ENDOR spectrum could arise from a single proton, if the tensors for the proton hyperfine and EPR anisotropy (g or ^{55}Mn hyperfine) are rhombic and noncoaxial (Hoffman et al., 1984). So inspection of the line shape of the spectrum does not reveal in general the number of different class of protons. However, from simulations of the EPR spectrum of MnCat(III,IV) we know that the g anisotropy is negligible and can be ignored (Zheng & Dismukes, 1992). ^{55}Mn hyperfine anisotropy is the source of the EPR line shape anisotropy. By performing ENDOR measurements in the center of the EPR signal (^{55}Mn, $|m_1| = |m_2| = {}^1/_2$) where the ^{55}Mn hyperfine anisotropy disappears, the resulting ^1H ENDOR spectra are expected to be simple powder line shapes of the ^1H hyperfine tensors. This is what we observed. The experimental ^1H ENDOR line shape in Figure 2 exhibits peaks which have opposite polarity on either side of the matrix peak, indicating that the principal components of the hyperfine tensors have different signs, i.e., $a_{iso} \ll |A_\parallel - A_\perp|$ (Kurreck et al., 1988). Thus, the protons interact with the electron spin through predominantly dipolar (spatial) rather than isotropic (Fermi-contact) interactions. From the intensities of the ENDOR peaks, we anticipated that there were at least two classes of anisotropic proton hyperfine tensors listed in Table I. Quantitative simulations using the model given next confirmed this assumption.

A quantitative model has been lacking for how to extract molecular structure information from ligand dipolar hyperfine interactions with a distributed spin system such as a paramagnetic cluster. The antiferromagnetic coupling that exists between the Mn ions in catalase and a number of other dimetalloproteins causes a significant change in both the magnitude and the direction of the internal magnetic field which the ligand nuclei feel. We have developed a theoretical model, implemented in a C program, which performs ENDOR simulations based on this model. The model considers the spin of each Mn ion, S_i, as localized at a separate point. This is the common point dipole approximation. It is an excellent approximation for ligand hyperfine couplings to Mn(II) but is expected to be less good for Mn(III) and Mn(IV), if there is appreciable spin transfer onto the ligands (covalency). The model considers that the Mn spins are coupled to produce a total spin $S = S_1 + S_2$. This gives a correct description of the spin of the ground state of this strongly coupled pair (Dismukes, 1991). We consider the possibility that both Mn ions exhibit hyperfine coupling [Fermi contact (a) and dipolar] to each ligand nucleus. The derivation of this "spin-coupled point pair" model is provided in the Appendix, while the method of simulation is described in the supplementary material. Here we focus on applying the model to simulate the spectrum.

Chart III: Proton Coordinates Which Were Used for Simulation of the Experimental ^1H ENDOR Spectrum of Mn-Catalase

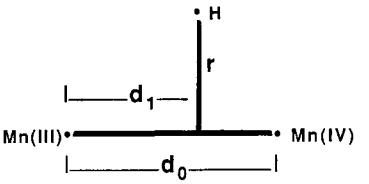

Table IV: Metrical Parameters,[a] Hyperfine Splittings,[b] and Deduced Hyperfine Proton Coordinate Sets Which Simulate the Experimental ENDOR Spectrum of Mn-Catalase

case	a_{iso}	a_1	a_2	a_3	r	d_1	r_1	r_2
I(a)	+0.93	+5.67	−3.93	−1.73	3.6	1.2	3.8	3.9
I(b)	−0.93	−5.67	+3.93	+1.73	2.75	3.7	4.6	2.9
II(a)	+1.47	5.13	−4.47	−0.67	3.45	2.0	4.0	3.5
II(b)	−1.47	−5.13	+4.47	+0.67	3.1	3.0	4.3	3.1

[a] Metrical parameters are given in angstroms. [b] Hyperfine splittings are given in megahertz.

The spectral simulations were performed by first expressing the internal coordinates (r_1, θ_1, r_2, and θ_2) of the three spins in terms of a single axis system originating on the proton. This transformation of the variables gives an expression that may then be solved for the dipolar magnetic field strength at any distance and any angle to the applied external field (Appendix and Chart III). For all simulations the Mn–Mn separation d_0 was fixed at 2.7 Å, the distance found in complexes possessing the $Mn_2(\mu\text{-}O)_2^{3+}$ core, and also determined by Mn EXAFS from the *L. plantarum* enzyme (Waldo et al., 1992). Simulation of the line shape for the three major pairs of ^1H ENDOR peaks in Figure 2 could be obtained for only a limited range of coordinates. We found the two cases listed in Table IV and diagramed in Chart IV. Since we do not know the signs of the ^1H hyperfine tensor parameters each case gives two sign choices, noted as (a) and (b), which have identical spectra. Both case I and II yield similar spectra. The case I(a,b) simulation is given in Figure 8b. It corresponds to parameters $r = 3.6$ Å, $d_1 = 1.2$ Å, and $a_{iso} = +0.93$ MHz for case I(a) or $r = 2.75$ Å, $d_1 = 3.7$ Å, and $a_{iso} = -0.93$ MHz for case I(b).

The location of the exchangeable proton for case I(a) is nearly equidistant from the two Mn ions. This suggests it may originate from a water molecular forming a distant (weak) H-bond to one or both μ-oxo atoms bridging between the Mn ions. A di-μ-oxo bridge has been predicted on the basis of the strong antiferromagnetic coupling of the Mn ions (Khangulov et al., 1986) and the short Mn–Mn distance (Waldo et al., 1992). The structures of several di-μ-oxo-dimanganese-(III,IV) complexes are well established. They all have Mn–Mn distances close to 2.7 Å and O–O distances within the planar Mn_2O_2 rhombus of 2.2–2.4 Å. Assuming this to be true for superoxidized MnCat, we would place the case I(a)

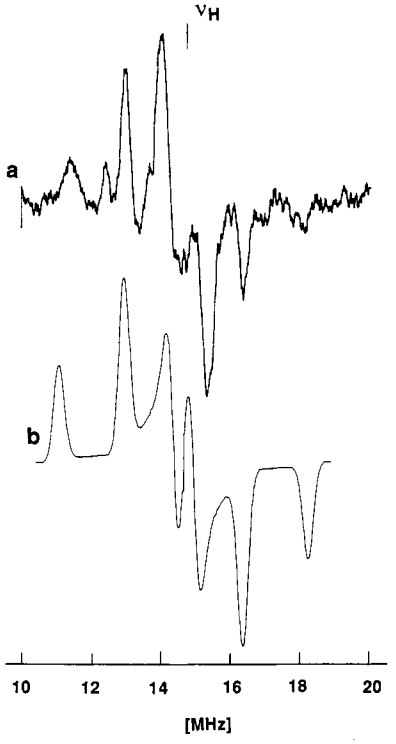

FIGURE 8: (a) ^{1}H ENDOR signal of catalase (Figure 2a) after subtraction of the central matrix peak. (b) Simulated ^{1}H ENDOR spectrum: $S_{1z} = 1$ for Mn(III) and $S_{2z} = -1/2$ for Mn(IV), $d_0 = 2.7$ Å, $r = 3.6$ Å, $d_1 = 1.2$ Å, and $a_{iso} = +0.93$ MHz (see text).

proton no closer than 2.3–2.4 Å to μ-O. The location of the proton for case I(b) is 1 Å outside of the Mn–Mn bisector closer to the Mn(IV) ion and 2.75 Å from the Mn–Mn vector (Chart IV). This case would arise if we chose the opposite sign for the hyperfine tensor. This results in a negative value for the largest dipolar hyperfine tensor component, as noted in Table IV.

Case II(a) corresponds to a proton located 0.5 Å closer to the Mn(IV) ion than to the Mn(III) ion. Compared to case I(a) it is slightly closer to the Mn–Mn projection vector at r = 3.45 Å. This location might arise from a water molecule H-bonded either to a μ-carboxylate bridge or possibly to a terminal carboxylate bound to Mn(IV). Case II(b) predicts the largest dipolar tensor component to have a negative hyperfine value of –1.47 MHz.

To help distinguish the cases illustrated in Chart IV, we observed angle-selected proton ENDOR data, which could test this assumption as follows. The ^{1}H ENDOR spectrum was recorded at the perpendicular turning point of the outer transition of the EPR spectrum noted in Figure 1a. Only two pairs of lines were observed at 0.8 and 3.3 MHz. According to our simulations of the EPR spectra of complex **1a** and several other di-μ-oxo complexes, the EPR intensity at the perpendicular turning point arises from molecules oriented with the plane of the $Mn_2(\mu\text{-}O)_2$ rhombus oriented parallel to the applied magnetic field.

To simulate the ^{1}H ENDOR signal at the perpendicular EPR turning point, we modified the simulation program to include ^{1}H ENDOR resonances only from molecules with the $Mn_2(\mu\text{-}O)_2$ plane located parallel to the external magnetic field (±3°). We performed simulations assuming different positions of the hydrogen atom. The first set of four simulations (not shown) were performed with the proton located in the $Mn_2(\mu\text{-}O)_2$ plane. In all four cases the simulated spectra reveal two line pairs of comparable intensities at 3.3- and 6.6-MHz separation. The latter coupling is not observed

Chart IV: Position of Hydrogen Atom Calculated for Different a_{iso} Values Presented in Table IV

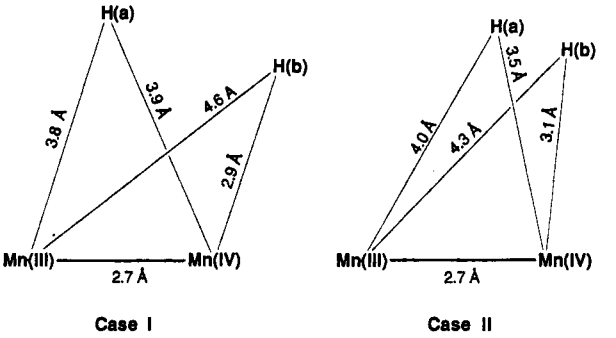

Chart V: Possible Localization of the OH Fragment from the D_2O Exchangeable Water (Hydroxide) Molecule Relative to $Mn_2(\mu\text{-}O)_2$ Plane of Mn-Catalase(III,VI) from *T. thermophilus* in Mn_2(III,IV)

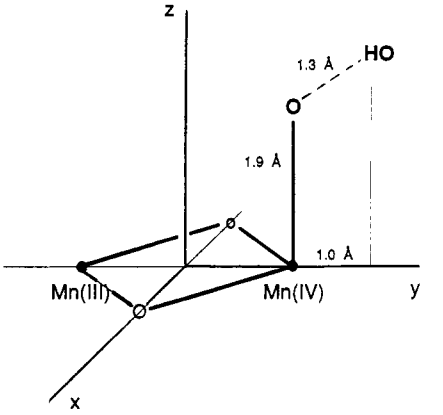

experimentally in the perpendicular spectrum (Figure 3a). None of these locations predicted the central line pair observed at 0.8 MHz (Figure 3a). A second set of four simulations also adopted the same positions of the H atom relative to the Mn–Mn vector as given by the four cases in Chart IV. However, the Mn–H–Mn plane was assumed to be perpendicular to the plane of the $Mn_2(\mu\text{-}O)_2$ rhombus. In this case the simulated spectra are extremely sensitive to the position of the H atom (Figure 3b–e). A reasonably close fit is obtained for Case I(b), as shown in Figure 3b, which predicts correctly the couplings of 0.8 and 3.3 MHz. Note that none of these latter cases predict the 6.6-MHz coupling, which must then correspond to a ^{1}H hyperfine tensor component oriented preferentially perpendicular to the $Mn_2(\mu\text{-}O)_2$ plane. Chart V summarizes these results along with a possible model for hydrogen bonding of this H atom to a terminal Mn(IV) oxygen ligand atom. Since the proton originates from a site which is both D_2O-exchangeable and displaced by ammonium sulfate, we ascribe it to a water (or hydroxide) molecule. Using a typical Mn(IV)–O bond length of 1.9 Å (Dutta et al., 1991) and assuming the hydrogen is located in the Mn–Mn–O_t plane, this would place the H atom at a distance no closer than 1.3 Å to O_t. This is compatible with a H-bonding interaction to a terminal or bridging carboxylate oxygen (Stoufer & Palenik, 1972; Wieghardt et al., 1987; Bashkin et al., 1988). Recently it was demonstrated that azide perturbs the EPR signal of catalase from *L. plantarum* in the Mn_2(III,IV) state (Penner-Hahn et al., 1992). We suggest that in this case the H-bonded water molecule is replaced by azide.

The H atom in case (b) possesses an isotropic hyperfine constant (a_{iso}) of –0.93 MHz. a_{iso} can be expressed as $a_{iso} = a_1P_1 + a_2P_2$ (Hendrich et al., 1992; see also Appendix, eq A5b), where a_1 and a_2 are the intrinsic isotropic hyperfine

constants for interaction with the Mn(III) and Mn(IV) ions, respectively. For case I(b) the distance between the proton and Mn(III) and Mn(IV) is 4.6 and 2.9 Å, respectively. Thus we may reasonably assume that the isotropic hyperfine interaction to Mn(IV) predominates with $|a_1| \ll |a_2|$. Taking into account that $P_2 = -1$ for Mn(IV) (see Appendix), we have $a_2 = +0.9$ MHz. The sign and magnitude of this isotropic interaction are close to the value of +0.8 MHz observed for water ligands to Mn(II) in $[Mn(H_2O)_6]^{2+}$ in frozen aqueous solutions, where the Mn–H distance is in the range 2.87 Å (Sivaraja & Dismukes, 1992). Elementary bonding considerations expect a directly coordinated water (or hydroxide) molecule bound to Mn(IV) to exhibit a much larger isotropic hyperfine interaction than for Mn(II). This is additional evidence that the proton with largest coupling in Mn-catalase originates from a H-bonded water (or hydroxide) molecule rather than a directly coordinated water (or hydroxide) molecule.

It is also possible in principle to explain the three major hyperfine couplings in Figure 2a by a more complex model in which two protons are located at terminally coordinated ligands where coupling to only one Mn ion occurs. Since each proton would then exhibit an axial line shape, this would require at least two protons with hyperfine couplings differing by a factor of about 2. A third proton would be required to account for the remaining peaks at 0.8 and 1.4 MHz. This model is disfavored on the basis of greater complexity and the need for more protons than are consistent with the EPR line width.

Comparison to Other Dimetalloenzymes. The spectroscopically deduced ligand coordination structure of MnCat(III,IV) from *T. thermophilus* appears to resemble the diiron(III) site of ribonucleotide reductase (RR) given in Chart I. The structures differ by the probable existence of a $(\mu\text{-O})_2$ linkage and one or both His ligands replaced by carboxylates in MnCat(III,IV), while RR possesses a single μ-O bridge. One could imagine that dehydration of one of the two water molecules bound to the Fe(III) ions of RR could form a second μ-O bridge. This should be favored for the higher oxidation state of Mn_2(III,IV) (Wieghardt, 1989). The existence of a $(\mu\text{-O})_2$ bridge in MnCat(III,IV) from *L. plantarum* seems very probable on the basis of Mn EXAFS results demonstrating a short 2.67-Å Mn–Mn distance (Waldo et al., 1992). On the basis of the EXAFS analysis, these authors suggest that MnCat from *L. plantarum* has a coordination structure like the polyhistidine coordination found in hemerythrin. Thus there appears to be either a major difference in the ligands to MnCat from the two organisms or a disagreement in the interpretation of the EXAFS and ENDOR experiments.

Although hemerythrin and Mn-catalase from *T. thermophilus* share very similar protein folds characterized by the four-helix bundle motif, their similarity appears to end there. The ENDOR data show clearly that the protein coordination of Mn in catalase resembles more closely the diiron site found in ribonucleotide reductase than it does that found for the diiron site in hemerythrin, Chart I. However, unlike the diiron(III) form of ribonucleotide reductase, there is no evidence for protonated water molecules bound directly to Mn ions of the catalase in Mn_2(III,IV) oxidation state. It will be of interest to compare the protein sequences once the catalase sequence becomes available.

The importance of the protein ligands in determining the allowed chemistry is illustrated extremely well by this comparison. Hemerythrin utilizes histidine ligands to stabilize the reduced form of Fe(II) to perform the nonredox function of reversible O_2 binding. Mn-catalase utilizes carboxylato ligands, which enable cycling between two oxidation states which must be close enough in redox potential that hydrogen peroxide can rapidly ($>10^7$ M^{-1} s^{-1}) oxidize one and reduce the other. Metal substitution studies on myohemerythrin have shown that replacement of both Fe(II) ions by Mn(II) abolishes the native O_2-binding activity and also fails to generate an active catalase (D, Kurtz, personal communication). The latter result was attributed to the difficulty in oxidizing the Mn(II) ions. This concept of protein coordination setting the redox potential is widely observed in electron transfer proteins. For MnCat it is not known if electron transfer, proton transfer, or peroxo chemistry is the origin of the rate-limiting step.

The spin-coupled point pair model can be applied easily to other dinuclear clusters to extract metrical information. There are only a few examples for which well-resolved ^{1}H ENDOR spectra have been reported. For example, there is a striking correspondence between the ^{1}H ENDOR coupling for D_2O-exchangeable protons in Mn-containing catalase (this work) and the diiron site of uteroferrin, as noted in Table I (Doi et al., 1988). Uteroferrin is an acid phosphatase which contains a spin-coupled pair of iron atoms. The ^{1}H ENDOR spectrum has been reported for the oxidation state Fe_2(II,III). This has a ground spin state $\mathbf{S} = \mathbf{S}_1 + \mathbf{S}_2 = {}^1/_2$ arising from the coupling of high-spin ions with $S_1 = {}^5/_2$ and $S_2 = 2$. The effective spins which need to be used in eq 4 to account for the antiferromagnetic coupling are (Dismukes, 1991) $\mathbf{S}_{1z} = {}^7/_6$ for Fe(II) and $\mathbf{S}_{2z} = -{}^4/_6$ for Fe(III), compared to $\mathbf{S}_{1z} = 1$ and $\mathbf{S}_{2z} = -{}^1/_2$ for Mn-catalase. Using these effective spins and the spin-coupled pair model, we can determine the distance for the proton with the largest hyperfine tensor in uteroferrin (Table I). The simulation indicates four possible positions, similar to the cases given for MnCat(III,IV) in Chart IV, but at a smaller distance. For example, for case I(a), distances Fe(II)–H and Fe(III)–H are 3.75 and 3.75 Å, respectively.

ACKNOWLEDGMENT

We are extremely grateful to Ms. T. Nekrassova for writing the C source code for the ENDOR simulation program and Mr. P. Pessiki for synthesis of complex 1. Drs. J. Sheats and M. Baumgarten provided important insight from unpublished studies on model complexes.

APPENDIX

Derivation of a "Spin-Coupled Point Pair Model" for Ligand Hyperfine Interactions with a Spin-Coupled Pair of Paramagnetic Ions. The antiferromagnetic coupling that exists between the Mn ions in catalase and a number of other dimetalloenzymes causes a significant change in both the magnitude and the direction of the internal magnetic field which the ligand nuclei feel. We consider a model in which the spin of each Mn ion, $\mathbf{S}_i$, is localized at a point and with the spins strongly coupled to produce a total spin $\mathbf{S} = \sum_i \mathbf{S}_i$. We consider the possibility that both Mn ions exhibit hyperfine coupling to each ligand nucleus. The expression for the hyperfine interactions between a set of nuclear spins, I_k, and a pair of electron spins coupled together by the Heisenberg exchange interaction is given by

$$H = J\mathbf{S}_1\cdot\mathbf{S}_2 + \sum_k^{\text{nuclei}} (\mathbf{S}_1\cdot a_{1k} + \mathbf{S}_2\cdot a_{2k})\mathbf{I}_k \qquad \text{(A1)}$$

In the presence of a strong external magnetic field defining the "Z axis" the electron and nuclear spins become oriented and the hyperfine interaction for each nucleus k may be simplified to eq A2a. This hamiltonian ignores off-diagnonal

hyperfine terms which are separated by energy of order J.

$$H = JS_1\cdot S_2 + (a_{1k}S_{1z} + a_{2k}S_{2z})\mathbf{I}_{kz} \quad \text{(A2a)}$$

$$H = {}^1/_2 J_{12}(\mathbf{S}^2 - \mathbf{S}_1{}^2 - \mathbf{S}_2{}^2) + (a_{1k}P_1 + a_{2k}P_2)\mathbf{S}_z\mathbf{I}_{kz} \quad \text{(A2b)}$$

$$\mathbf{S}_{1z} = P_1\mathbf{S}_z = \mathbf{S}_1\cdot\mathbf{S}/\mathbf{S}^2 = \frac{[S(S+1) + S_1(S_1+1) - S_2(S_2+1)]}{2S(S+1)}\mathbf{S}_z \quad \text{(A3)}$$

Equation A2b is obtained using the Wigner–Echart theorem (Tinkham, 1964). This enables evaluation of the individual spin operators like $\mathbf{S}_{1z}$ and $\mathbf{S}_{2z}$, using the total spin angular momentum states as a basis, $|\mathbf{S},\mathbf{S}_z,\mathbf{S}_1,\mathbf{S}_2|$. the latter basis diagonalizes the much larger spin exchange term. Equation A3 gives the vector coupling coefficient, expressed as the projection P_1, needed to express the individual ion electron spin in terms of the total spin of the dimer. P_2 is obtained by exchanging labels 1 and 2. It should be emphasized that eqs A2 and A3 are not approximations other than the assumption of a strong external magnetic field. The conditions under which eq A3 may be used have been summarized elsewhere (Dismukes, 1991). This shows that the ligand hyperfine interactions for Mn(III) and Mn(IV) ions in a spin-coupled cluster are scaled from those of the isolated ion value by $P_1 = 2$ and $P_2 = -1$, respectively. This scales both the isotropic Fermi contact (a) and dipolar hyperfine (T) contributions to the hyperfine tensors. The net hyperfine interaction given by the second term in eq A2 can be expanded by using explicit expressions for the contact and dipolar hyperfine terms, as shown in (Carrington & McLachlan, 1967):

$$E(M_s,M_k) = \{[a_1 - g\beta g_n\beta_n\langle(\mathbf{r}_1{}^2 - 3\mathbf{z}^2)/\mathbf{r}_1{}^5\rangle]P_1 + [a_2 - g\beta g_n\beta_n\langle(\mathbf{r}_2{}^2 - 3\mathbf{z}^2)/\mathbf{r}_2{}^5\rangle]P_2\}M_sM_k \quad \text{(A4)}$$

Here $\mathbf{r}_i$ is a vector directed from the electron spin of manganese ion i to a magnetic ligand atom. Evaluation of eq A4 requires that a spatial average of the total electronic spin be performed.

To continue further we will make an approximation. We treat the two electron spins as point magnetic sources localized at each Mn nucleus, but still coupled by the spin-exchange interaction—the "spin-coupled point pair" model. This reduces eq A4 to eq A5, which requires no spatial integration of the spin density other than to split it into two point sources:

$$E(M_s,M_k) = \{[a_1 - g\beta g_n\beta_n(3\cos^2\theta_1 - 1)/|\mathbf{r}_1|^3]P_1 + [a_2 - g\beta g_n\beta_n(3\cos^2\theta_2 - 1)/|\mathbf{r}_2|^3]P_2\}M_sM_k \quad \text{(A5a)}$$

The vectors $\mathbf{r}_1$ and $\mathbf{r}_2$ make angles θ_1 and θ_2 with the unit vector $\mathbf{z}$ parallel to the external magnetic field direction. The correct values of the electron spins to use in eq A5 are not the isolated ion values of 2 and ${}^3/_2$. Rather, for the case of an $S = {}^1/_2$ state they are $\mathbf{S}_{1z} = P_1M_s = 1$ for Mn(III) and $\mathbf{S}_{2z} = P_2M_s = -{}^1/_2$ for Mn(IV).

Considering the case for nuclei with spins $I = {}^1/_2$, the ENDOR frequencies (ν) for the nuclear transition $\Delta M_k = 1$ for the upper and lower electron spin states ($\pm{}^1/_2$) are obtained from eq A5a by adding the nuclear Zeeman frequency, ν_H, for the case of protons. For simplicity in the simulation of the ENDOR spectra we use a single isotropic hyperfine parameter which can be separated into the contributions from the individual Mn ions:

$$a = a_1P_1 + a_2P_2 \quad \text{(A5b)}$$

This gives eq A6 for the ENDOR frequencies:

$$\nu = |\nu_H \pm ({}^1/_h)\{a - [g\beta g_n\beta_n(3\cos^2\theta_1 - 1)/|\mathbf{r}_1|^3]P_1 - [g\beta g_n\beta_n(3\cos^2\theta_2 - 1)/|\mathbf{r}_2|^3]P_2\}| \quad \text{(A6)}$$

Spectral simulations are much easier to perform by first expressing the coordinates of the three spins in a new axis system which enables assignment of the internal coordinates such as the Mn–Mn separation (Chart III). In terms of an axis system with the H atom located at the origin, the location of the Mn–Mn vector $\mathbf{d}_0$ may be described as follows. The vector $\mathbf{r}$ is drawn from the origin to the point along $\mathbf{d}_0$ which defines the normal to $\mathbf{d}_0$. This point is choosen to be in the yz plane for convenience. The distance from this intersection point to Mn_1(III) is given by $\mathbf{d}_1$ and to Mn_2(IV) is given by $\mathbf{d}_2 = \mathbf{d}_0 + \mathbf{d}_1$. The orientation of the Mn–Mn vector relative to the origin is described by two angles θ and α. θ is the angle between the laboratory $\mathbf{z}$ axis defined by the external magnetic field and $\mathbf{r}$. α is the angle between $\mathbf{d}_0$ and its projection into the yz plane.

With these definitions, eq A6 may be rewritten using the following expressions for θ_1, θ_2, r_1 and r_2:

$$\cos^2\theta_i = [(\mathbf{r}_i\cdot\mathbf{z})/|\mathbf{r}_i|]^2 - \sin^2\gamma_i\cos^2\theta + \cos^2\gamma_i\sin^2\theta\cos^2\alpha + {}^1/_2\sin 2\gamma_i\sin 2\theta\cos\alpha$$

$$\sin^2\gamma_i = r_i^2/(d_i^2 + r_i^2)$$

$$\cos^2\gamma_i = d_i^2/(d_i^2 + r_i^2)$$

$$r_i = (d_i + r)^{1/2}$$

To compute the spectral intensity for a randomly oriented "powder" sample as a function of frequency, each transition predicted by eq A6 was multiplied by the probability for a given θ and α orientation arising, $P(\theta,\alpha) = \sin\theta$, and by a Gaussian line width function $g(\nu - \nu')$ and integrated over θ and α, as described by

$$I(\nu) = \int_0^\pi d\alpha \int_0^\pi g(\nu - \nu')\sin\theta\, d\theta \quad \text{(A7a)}$$

$$E(\nu) = dI(\nu)/d\nu \quad \text{(A7b)}$$

where $E(\nu)$ is the frequency-modulated ^{1}H ENDOR spectrum. Equations A6 and A7 were used to simulate the experimental ^{1}H ENDOR spectra.

SUPPLEMENTARY MATERIAL AVAILABLE

A description and one figure illustrating the simulation strategy used to search for the locations of protons which could reproduce the experimental ENDOR spectra (2 pages). Ordering information is given on any current masthead page.

REFERENCES

Abragam, A., & Bleaney, B. (1970) *Electron Paramagnetic Resonance of Transition Ions*, Clarendon Press, Oxford, England.

Babcock, G. T. (1987) in *New Comprehensive Biochemistry* (Amesz, J., Ed.) pp 125–158, Elsevier, Amsterdam.

Barynin, V. V., & Grebenko, A. I. (1986) *Dokl. Acad. Nauk SSSR 286*, 461–464 (Russian).

Barynin, V. V., Vagin, A. A., Melik-Adamyan, V. R., Grebenko, A. I., Khangulov, S. V., Popov, A. N., Andrianova, M. E., & Vainshtein, B. K. (1986) *Dokl. Akad. Nauk SSSR 288*, 877–880 (Russian).

Bashkin, J. S., Schake, A. R., Vincent, J. B., Chang, H.-R., Li, Q., Huffman, J. C., Chrisrou, G., & Hendrickson, D. N. J. (1988) *J. Chem. Soc., Chem. Commun.*, 700–702.

Beer, R., De Boer, W., van't Hoff, V., & Ormondt, V. (1972) *Acta Crystallogr. B29*, 1473.

Beyer, W. F., & Fridovich, I. (1985) *Biochemistry 24*, 6460–6467.

Britt, R. D. (1988) Ph.D. Thesis [Lawrence Berkeley Laboratory, Report LBL-25042], Department of Physics, University of California, Berkeley, CA.

Brudvig, G. W., Beck, W. F., & dePaula, J. C. (1989) *Annu. Rev. Biophys. Biophys. Chem. 18*, 25–46.

Carrington, A., & McLachlan, K. (1967) in *Introduction to Magnetic Resonance*, pp 103–106, Harper and Row, New York.

Christen, D., Griffiths, J. H., & Sheridan, J. (1982) *Z. Naturforsch. 37a*, 1378–1385.

Cooper, S. R., Dismukes, G. C., Klein, M. P., & Calvin, M. C. (1978) *J. Am. Chem. Soc. 100*, 7248–7252.

Dikanov, S. A., Tsevetkov, Yu. D., Khangulov, S. V., & Goldfeld, M. G. (1988) *Dokl. Biophys. (Engl. Transl.) 302*, 107–206.

Diril, H., Chang, H.-R., Nilges, M. J., Zhang, X., Potenza, J. A., Schugar, H. J., Isied, S. S., & Hendrickson, D. N. (1989) *J. Am. Chem. Soc. 111*, 5102–5114.

Dismukes, G. C. (1988) *Chem. Scr. 28A*, 99–104.

Dismukes, G. C. (1991) Mixed Valency and Vibronic Trapping in Multinuclear Manganese Enzymes and Clusters, in *Mixed Valency Systems: Applications in Chemistry, Physics and Biology* (Prassides, K., Ed.) pp 137–154, Kluwer Academic Publishers, Dordrecht, The Netherlands.

Dismukes, G. C. (1992) Polynuclear Manganese Enzymes, in *Bioinorganic Catalysis* (Reedijk, J., Ed.) pp 317–346, Marcel-Dekker, Amsterdam.

Dismukes, G. C., Sheats, J. E., & Smegal, J. A. (1987) *J. Am. Chem. Soc. 109*, 7202–7203.

Doi, K., McCracken, J., Peisach, J., & Aisen, P. (1988) *J. Biol. Chem. 263*, 5757–5763.

Fronko, R. M., Penner-Hahn, J. E., & Bender, C. J. (1988) *J. Am. Chem. Soc. 110*, 7555–7556.

Hansson, O., & Wydrzynski, T. (1990) *Photosynth. Res. 23*, 131–162.

Hendrich, M. P., Fox, B. G., Andersson, K. K., Debrunner, P. G., & Lipscomb, J. D. (1992) *J. Biol. Chem. 267*, 261–269.

Hoffman, B. M., Martinsen, J., & Venters, R. A. (1984) *J. Magn. Reson. 59*, 110–123.

Hoffman, B. M., Martinsen, J., & Venters, R. A. (1985) *J. Magn. Reson. 62*, 537–542.

Jorin, E., Schweger, A., & Gunthard, Hs. H. (1980) *Chem. Phys. Lett. 69*, 193–197.

Khangulov, S. V., Barynin, V. V., Melik-Adamyan, V. R., Grebenko, A. I., Voevodskay, N. V., Blumenfeld, L. A., Dobrykov, S. N., & Il'ysova, V. B. (1986) *Bioorg. Khim. 12*, 741–748 (Russian).

Khangulov, S. V., Voevodskaya, N. V., Barynin, V. V., Grebenko, A. I., & Melik-Adamyan, V. R. (1987) *Biofizika 32*, 960–966 (Russian).

Khangulov, S. V., Andreeva, N. E., Gerasimenko, V. V., Goldfeld, M. G., Barynin, V. V., & Grebenko, A. I. (1990a) *Russ. J. Phys. Chem. (Engl. Transl.) 64*, 10–16.

Khangulov, S. V., Barynin, V. V., & Antonyuk-Barynina, S. V. (1990b) *Biochim. Biophys. Acta 1020*, 25–33.

Khangulov, S. V., Goldfeld, M. G., Gerasimenko, V. V., Andreeva, N. E., Barynin, V. V., & Grebenko, A. I. (1990c) *J. Inorg. Biochem. 40*, 279–292.

Khangulov, S. V., Barynin, V. V., Voevodskaya, N. V., & Grebenko, A. I. (1990d) *Biochim. Biophys. Acta 1020*, 305–310.

Kono, Y., & Fridovich, I. (1983a) *J. Biol. Chem. 258*, 6015–6019.

Kono, Y., & Fridovich, I. (1983b) *J. Biol. Chem. 258*, 13646–13648.

Kurreck, H., Kirste, B., & Lubitz, W. (1988) *Electron Nuclear Double Resonance Spectroscopy of Radicals in Solution*, p 41, VCH Publishers, New York.

Lebedev, Ya. S., & Muromtcev, V. I. (1972) *EPR Relaxation of Stabilized Radicals*, p 43, Publisher Khimiya, Moscow.

Nordlund, P., Sjoberg, B.-M., & Eklund, H. (1990) *Nature 345*, 593–598.

Que, L., Jr., & True, A. E. (1990) *Progress in Inorganic Chemistry: Biorganic Chemistry 38* (Lippard, S. J., Ed.) p 97, John Wiley & Sons, Inc., New York.

Ragle, J. L., & Minott, G. L. (1978) in *Advances in Nuclear Quadrupole Resonance* (Smith, J. A. S., Ed.) Vol. 3, Heyden Publisher, London, Philadelphia, PA, and Rheine.

Rist, G. H., & Hyde, J. S. (1970) *J. Chem. Phys. 52*, 4633–4643.

Scholes, C. P., Lapidot, A., Mascarenhas, R., Inubushi, T., Isaacson, R. A., & Feher, G. (1982) *J. Am. Chem. Soc. 104*, 2724–2735.

Scholes, C. P., Falkowski, K. M., Chen, Sh., & Bank, (1986) *J. Am. Chem. Soc. 108*, 1660–1671.

Sieker, L. C., Stemkamp, R. E., & Jensen, L. H. (1982) in *The Biological Chemistry of Iron* (Dunford, H. B., Dolphin, D., Raymond, K. S., & Sieker, L. C., Eds.) pp 161–175, D. Riedel, New York.

Sivaraja, M., Stouch, T. R., & Dismukes, G. C. (1992) *J. Am. Chem. Soc. 114*, 9600–9603.

Stoufer, A., & Palenik, G. (1972) *J. Am. Chem. Soc. 94*, 2121–2123.

Tan, X.-l., Gultneh, Y., Sarneski, J. E., & Scholes, C. P. (1991) *J. Am. Chem. Soc. 113*, 7853–7858.

Tinkham, M. (1964) *Group Theory and Quantum Mechanics*, p 131, McGraw-Hill, New York and London.

Vainshtein, B. K., Melik-Adamyan, V. R., Barynin, V. V., & Vagin, A. A. (1984) in *Progress in Bioorganic Chemistry and Molecular Biology* (Ovchinnikov, Yu., Ed.) pp 117–132; Elsevier, Amsterdam, New York, and Oxford, England.

Vainshtein, B. K., Melik-Adamyan, V. R., Barynin, V. V., Vagin, A. A., & Grebenko, A. I. (1985) *Proc. Int. Symp. Biomol. Struct. Interact., Suppl. J., Biosci. 8* (1 and 2), 471–479.

Vanngard, T., Hansson, O., & Haddy, O., & Haddy, A. (1992) in *Manganese Redox Enzymes* (Pecoraro, V. L., Ed.) pp 105–118, VCH Publishers, Inc., New York.

Waldo, G. S., Fronko, R. M., & Penner-Hahn, J. E. (1991) *Biochemistry 30*, 10496–10490.

Waldo, G. S., Yu, S., & Penner-Hahn, J. E. (1992) *J. Am. Chem. Soc. 114*, 5869–5870.

Wieghardt, K. (1989) *Angew. Chem., Int. Ed. Engl. 28*, 1153–1172.

Wieghart, K., Bossek, U., Zsolnai, L., Huttner, G., Blondin, G., Girerd, J.-J., & Babonneau, F. (1987) *J. Chem. Soc., Chem. Commun.* 651–653.

Willing, A., Follmann, H., & Auling, G. (1988) *Eur. J. Biochem. 170*, 603–611.

Zheng, M., & Dismukes, G. C. (1992) in *Proceedings of the 9th International Congress on Photosynthesis* (Murata, N., Ed.) pp 305–308, Kluwer Academic Publishers, Dordrecht, The Netherlands.